

# NJC

Accepted Manuscript



This is an *Accepted Manuscript*, which has been through the Royal Society of Chemistry peer review process and has been accepted for publication.

*Accepted Manuscripts* are published online shortly after acceptance, before technical editing, formatting and proof reading. Using this free service, authors can make their results available to the community, in citable form, before we publish the edited article. We will replace this *Accepted Manuscript* with the edited and formatted *Advance Article* as soon as it is available.

You can find more information about *Accepted Manuscripts* in the [Information for Authors](#).

Please note that technical editing may introduce minor changes to the text and/or graphics, which may alter content. The journal's standard [Terms & Conditions](#) and the [Ethical guidelines](#) still apply. In no event shall the Royal Society of Chemistry be held responsible for any errors or omissions in this *Accepted Manuscript* or any consequences arising from the use of any information it contains.

## ARTICLE

# Gold nanoparticles-sensitized wide and narrow band gap TiO<sub>2</sub> for visible light applications: A comparative study<sup>†</sup>

Cite this: DOI: 10.1039/x0xx00000x

Received 00th January 2012,  
Accepted 00th January 2012

DOI: 10.1039/x0xx00000x

[www.rsc.org/](http://www.rsc.org/)Sajid Ali Ansari,<sup>a</sup> Mohammad Mansoob Khan,<sup>ab\*</sup> Mohd Omaish Ansari<sup>a</sup> and Moo Hwan Cho<sup>a\*</sup>

Gold nanoparticles (AuNPs)-sensitized wide band gap TiO<sub>2</sub> (Au/P-TiO<sub>2</sub>) and narrow band gap TiO<sub>2</sub> (Au/M-TiO<sub>2</sub>) nanocomposites were prepared using an electrochemically active biofilm. The optical and structural properties of the Au/P-TiO<sub>2</sub> and Au/M-TiO<sub>2</sub> nanocomposites were characterized using standard techniques. The surface plasmon resonance (SPR) absorption characteristics of the AuNPs on the TiO<sub>2</sub> surface extended the absorption edge of P-TiO<sub>2</sub> and M-TiO<sub>2</sub> to the visible light region. The photocatalytic activity of the Au/P-TiO<sub>2</sub> and Au/M-TiO<sub>2</sub> nanocomposites were evaluated by the photodegradation of methylene blue, methyl orange dyes and 2-chlorophenol under visible light irradiation, where Au/M-TiO<sub>2</sub> nanocomposites exhibited enhanced photocatalytic activity compared to the Au/P-TiO<sub>2</sub> nanocomposite and P-TiO<sub>2</sub> and M-TiO<sub>2</sub> nanoparticles. Furthermore, the higher photoelectrochemical performance of the Au/M-TiO<sub>2</sub> nanocomposite compared to the Au/P-TiO<sub>2</sub> nanocomposite and P-TiO<sub>2</sub> and M-TiO<sub>2</sub> nanoparticles further support its higher visible light active behavior under visible light irradiation. The pronounced photoactivities of the Au/M-TiO<sub>2</sub> nanocomposite in the visible region were attributed to the interfacial synergistic effects of the two phenomena, i.e. the SPR effect of AuNPs and the defect-induced band gap reduction of M-TiO<sub>2</sub> nanoparticles. The present work provides a newer insight towards the development of nanocomposites of noble metals and defective metal oxides with high efficiency in the field of visible light-induced photoactivities.

## Introduction

The excessive use of organic chemicals in both industrial manufacturing and normal household uses have led to their leaching in the environment, leading to an alarming environmental contamination.<sup>1</sup> Organic chemicals are present as pollutants in ground water and surface water, such as wells, ponds and lakes.<sup>2</sup> To achieve drinking water quality, pollutants need to be removed to protect the water resources. Several processes, such as adsorption on supported substrates, ultrasonic irradiation, and electrochemical, biological and chemical oxidation,<sup>2,3,4</sup> have been used widely to destroy or remove these toxins. Among these techniques, the visible light photocatalytic detoxification of organic pollutants have attracted considerable attention for its many advantageous properties, such as the use of very small amounts of catalyst, regeneration of catalyst, utilization of natural sunlight for environmental remediation and clean energy production.<sup>5,6</sup>

These days, there has been extensive research efforts into the development of novel visible light active photocatalyst materials

with high efficiency.<sup>5-7</sup> Metal oxide nanostructures, such as TiO<sub>2</sub> and ZnO, have recently shown practical performance as effective photocatalysts utilizing solar light.<sup>5,7,8</sup> The metal oxide photocatalyst generally involves the in-situ production of strong oxidizing species of superoxide radical anions (<sup>•</sup>O<sub>2</sub><sup>-</sup>) and hydroxyl radicals (HO<sup>•</sup>), which triggers a sequence of reactions that ultimately breaks down the dye macromolecules into smaller and less harmful substances, leading to mineralization.<sup>5,6,8,9</sup> Among these, TiO<sub>2</sub> has been the prime choice for researchers worldwide owing its properties, such as low toxicity, low cost and high active surface area etc.<sup>5,10</sup> On the other hand, the photocatalytic efficiency of TiO<sub>2</sub> has limited use because of its poor utilization of solar energy (< 5% of the solar spectrum), which is due to its wide band gap (~3.2 eV) and rapid recombination rate of photoexcited charge carriers.<sup>10,11</sup>

Many studies have focused on improving the visible light response of TiO<sub>2</sub> nanoparticles by doping with metals or nonmetals, by fabricating a suitable textural design, and forming a nano-heterojunction by combining them with other metal oxide nanostructures.<sup>10-12</sup> Recently, defect engineering, which leads to the

introduction of defects, such as  $\text{Ti}^{3+}$  formation and/or oxygen vacancies, have been reported to be an effective way of reducing the band gap of  $\text{TiO}_2$  nanoparticles.<sup>13-15</sup> The merits of defects and vacancies are that it preserves the intrinsic crystal structure of  $\text{TiO}_2$  without introducing impurity elements, leading to enhanced photocatalytic performance under visible light irradiation.<sup>13-16</sup> Several efforts have been made for defect engineering of  $\text{TiO}_2$  nanoparticles, which involves a combustion method,<sup>17</sup> high pressure hydrogenation of  $\text{TiO}_2$ , hydrogen thermal treatment,<sup>18</sup> plasma treatment,<sup>19</sup> high energy particle bombardment etc.<sup>20</sup> On the other hand, most of these processes have their own advantages and disadvantages; they are limited by complicated procedures, high cost and cannot be considered as environmentally benign processes.

The other important aspect of photochemical reaction besides extending the light absorption range of  $\text{TiO}_2$  by defects ( $\text{Ti}^{3+}$  and/or oxygen vacancy) is to improve the charge separation efficiency.<sup>21</sup> The photosensitization of  $\text{TiO}_2$  with plasmonic noble metal nanostructures, such as gold nanoparticles (AuNPs) utilizes unique surface plasmon resonance (SPR) absorbance features of noble metal nanoparticles, which promotes charge separation and enhances light absorption.<sup>12,22-26</sup> Noble metal nanoparticles/ $\text{TiO}_2$  nanocomposites can effectively deter the recombination of photoexcited electron-hole pairs, thereby improving the photocatalytic performance of  $\text{TiO}_2$ .<sup>12,21,23</sup> Therefore, nanocomposites of AuNPs with  $\text{TiO}_2$  containing defects ( $\text{Ti}^{3+}$  and/or oxygen vacancy) are expected to show enhanced photocatalytic properties due to the synergistic effect, i.e., defects induce visible light absorption in  $\text{TiO}_2$  while the addition of a noble metal helps enhance the visible light absorption because of its SPR effect and ability to inhibit the recombination of photogenerated electron-hole pairs.<sup>12,22,23</sup>

In this study, AuNPs-sensitized wide band gap  $\text{TiO}_2$  (Au/P- $\text{TiO}_2$ ) and narrow band gap  $\text{TiO}_2$  (Au/M- $\text{TiO}_2$ ) nanocomposite photocatalysts were synthesized using an electrochemically active biofilm (EAB). The photocatalytic activities of the Au/P- $\text{TiO}_2$  and Au/M- $\text{TiO}_2$  nanocomposites were evaluated by the degradation of methylene blue (MB), methyl orange (MO) and 2-chlorophenol (2-CP) under visible light irradiation. The degradation efficiency was also compared with the pure  $\text{TiO}_2$  (P- $\text{TiO}_2$ ) and defect-induced narrow band gap  $\text{TiO}_2$  (M- $\text{TiO}_2$ ) nanoparticles. The enhancement of the visible light activity of Au/M- $\text{TiO}_2$  nanocomposite was evaluated further by the photoelectrochemical measurements, such as electrochemical impedance spectroscopy (EIS) and differential pulse voltammetry (DPV) in the dark and under visible light irradiation.

## Experimental

### Materials

Titanium dioxide nanoparticles ( $\text{TiO}_2$ ) were purchased from Degussa whereas MB and 2-CP were purchased from Sigma-Aldrich. Hydrogen tetrachloroaurate (III) hydrate ( $\text{HAuCl}_4 \cdot n\text{H}_2\text{O}$ ;  $n = 3.7$ ) was acquired from Kojima Chemicals, Japan. Sodium sulfate ( $\text{Na}_2\text{SO}_4$ ), sodium acetate ( $\text{CH}_3\text{COONa}$ ) and MO were obtained from Duksan Pure Chemicals Co. Ltd. South Korea. Ethyl cellulose and  $\alpha$ -terpineol were supplied by KANTO Chemical Co., Japan and fluorine-doped transparent conducting oxide glass (FTO; F-doped

$\text{SnO}_2$  glass;  $7 \Omega/\text{sq}$ ) was purchased from Pilkington, USA. Carbon paper (without wet proof, Fuel Cell Earth LLC, USA), and all other chemicals used in this study were of analytical grade and used as received.

### Methods

Phase characterization was accomplished by X-ray diffraction (XRD, PANalytical, X'pert PRO-MPD, Netherland), using  $\text{Cu K}\alpha$  radiation ( $\lambda = 0.15405 \text{ nm}$ ). The optical properties of the samples (Au/P- $\text{TiO}_2$  and Au/M- $\text{TiO}_2$  nanocomposites) were analyzed by ultraviolet-visible-near infrared (UV-VIS-NIR, Cary 5000, VARIAN, USA) spectrophotometry. The photoluminescence (PL, Kimon, 1 K, Japan) of the samples were recorded over the scanning range, 200-800 nm, with an excitation wavelength of 325 nm. The chemical state and surface composition was analyzed by X-ray photoelectron spectroscopy (XPS, ESCALAB 250 XPS System, Thermo Fisher Scientific U.K.) using a monochromatized  $\text{Al K}\alpha$  x-ray source ( $h\nu = 1486.6 \text{ eV}$ ). PL and XPS were conducted at the Korea Basic Science Institute (KBSI), South Korea. The size and distribution of the Au/P- $\text{TiO}_2$  and Au/M- $\text{TiO}_2$  nanocomposites were observed by field emission transmission electron microscopy (FE-TEM, Tecnai G2 F20, FEI, USA) with an accelerating voltage of 200 kV combined with energy dispersive spectrometry (EDS). The photoelectrochemical and photocatalytic experiments were performed using a 400 W lamp with an intensity of  $31 \text{ mW/cm}^2$  (3M,  $\lambda > 400 \text{ nm}$ , USA). The photoelectrochemical measurements are presented schematically in Fig. S1. EIS was performed using a three electrode cell with a 0.2 M  $\text{Na}_2\text{SO}_4$  aqueous solution as the electrolyte using a potentiostat (VersaSTAT 3, Princeton Research, USA). The DPV of the Au/P- $\text{TiO}_2$  and Au/M- $\text{TiO}_2$  nanocomposites photoelectrodes were recorded with a pulse height of 50 mV, pulse width of 0.005 s and scan rate of 4 mV/s. The working electrodes were prepared as follows. 100 mg of the Au/P- $\text{TiO}_2$  and Au/M- $\text{TiO}_2$  nanocomposites were suspended thoroughly using a mixer after adding ethyl cellulose as a binder and  $\alpha$ -terpineol as a solvent for the paste. The resulting mixture was then coated on a FTO glass electrode using the doctor-blade method. The Au/P- $\text{TiO}_2$  and Au/M- $\text{TiO}_2$  nanocomposite-coated (FTO) glass substrates were used as the working electrode. Ag/AgCl (3.0 M KCl) and a Pt gauge were used as the reference and counter electrodes, respectively.

### Natural development of electrochemically active biofilm in an anaerobic environment

EAB was developed on plain carbon paper according to previous reports.<sup>27-29</sup> In a typical process, a mineral salt medium containing sodium acetate (1 g/L) was prepared in a 250 mL glass bottle to which carbon paper, which acted as a growing support for EAB, was dipped. Subsequently, 10 mL of anaerobic sludge (from a biogas plant in Paju, Korea) was added under strict anaerobic conditions by sparging  $\text{N}_2$  gas for 5 min to create an inert atmosphere. All media, including the bacterial inoculum, were changed after two days under strict anaerobic conditions. This process was repeated over a two week period, which resulted in the formation of a uniform layer of a living EAB on the surface of the carbon paper.

## Synthesis of Au/P-TiO<sub>2</sub> and Au/M-TiO<sub>2</sub> nanocomposites

The EAB developed on plain carbon paper was used to synthesize the Au/P-TiO<sub>2</sub> or Au/M-TiO<sub>2</sub> nanocomposites, as shown in Fig. 1. The Au/M-TiO<sub>2</sub> nanocomposite involved two synthetic steps, first the modification of TiO<sub>2</sub><sup>13</sup> followed by the anchoring of AuNPs to the M-TiO<sub>2</sub> surface which is also similar to our previous reports.<sup>9,23</sup> In short, a 4 mM dispersion of M-TiO<sub>2</sub> was prepared in water. The 3 mM Au precursor was added to the above dispersion of M-TiO<sub>2</sub>. Subsequently, 0.2 g sodium acetate was added to the above mixture. The reaction mixture was stirred for 5 min to allow the proper adsorption of AuCl<sub>4</sub><sup>-</sup> ions on M-TiO<sub>2</sub> surface, after which the EAB formed on carbon paper was hung in the glass bottle. The EAB in this system is associated with the biological oxidation of sodium acetate, leading to the generation of excess of electrons, which assists in the reduction of Au<sup>3+</sup> ions to Au<sup>0</sup> on the surface of M-TiO<sub>2</sub>. The Au/P-TiO<sub>2</sub> nanocomposite was also synthesized similarly using P-TiO<sub>2</sub> nanoparticles instead of M-TiO<sub>2</sub> nanoparticles (Fig. 1).

Two control experiments were also performed to determine the roles of EAB and acetate.<sup>9,23</sup>

## Photocatalytic degradation experiments

The photodegradation efficiency of the Au/P-TiO<sub>2</sub> and Au/M-TiO<sub>2</sub> photocatalyst under visible light irradiation was examined by the decomposition of MB, MO, and 2-CP. In a simple photodegradation process, 2 mg of the Au/P-TiO<sub>2</sub> and Au/M-TiO<sub>2</sub> photocatalyst was dispersed in 20 mL of an aqueous MB, MO (10 mg/L), and 2-CP (30 mg/L) solution by stirring for 10 min in the dark to achieve adsorption-desorption equilibrium. The above suspensions were irradiated with visible light to degrade the MB, MO and 2-CP. After the start of the reaction, a 2 mL sample of the solution was taken every 1 h, from which the catalyst was separated by centrifugation. The absorbance of the above solution was analyzed by UV-vis spectrophotometry (Optizen 2120UV). The photodegradation efficiency of the Au/P-TiO<sub>2</sub> and Au/M-TiO<sub>2</sub> photocatalyst was calculated from the obtained absorbance data using the method reported elsewhere.<sup>13,15,23</sup>

## Photoelectrochemical studies (EIS and DPV)

The photoelectrochemical properties of the Au/P-TiO<sub>2</sub> and Au/M-TiO<sub>2</sub> nanocomposites in the dark and under visible light irradiation were analyzed by EIS and DPV experiments. The DPV experiment was carried out under ambient conditions in 50 mL of a 0.2 M phosphate buffer solution (pH = 7), whereas the EIS experiment was performed in 50 mL of an aqueous 0.2 M Na<sub>2</sub>SO<sub>4</sub> solution at room temperature.

## Results and discussion

### Characterization and photodegradation results of P-TiO<sub>2</sub> and M-TiO<sub>2</sub>

The formation of defects in M-TiO<sub>2</sub> (Ti<sup>3+</sup> formation and/or oxygen vacancies) has already been justified in our previous

reports.<sup>13</sup> Now we have added some relevant data such as XRD pattern, UV-visible absorption spectra, electron paramagnetic resonance (EPR) and XPS spectra in the electronic supplementary information for better understanding. The XRD pattern shows that the (101) peak of the M-TiO<sub>2</sub> was shifted to a lower angle compared to that of P-TiO<sub>2</sub> (Fig. S2a). The XRD peak shift towards a lower angle might be due to lattice expansion by the formation of Ti<sup>3+</sup> ions (the ionic radius of Ti<sup>3+</sup> is larger than that of Ti<sup>4+</sup>) in the M-TiO<sub>2</sub>.<sup>13</sup> The band gap of the P-TiO<sub>2</sub> and M-TiO<sub>2</sub> were estimated directly from the UV-visible absorption spectra (Fig. S2b), and found to be ~2.85 eV for the M-TiO<sub>2</sub>, which was red shifted compared to the P-TiO<sub>2</sub> (E<sub>g</sub> = 3.10 eV). The observed band gap of the M-TiO<sub>2</sub> was substantially smaller than that of the P-TiO<sub>2</sub> and was attributed to the presence of defects in M-TiO<sub>2</sub>.<sup>13,14,21,25</sup> The P-TiO<sub>2</sub> did not show any EPR signals (Fig. S2c), whereas the M-TiO<sub>2</sub> showed strong EPR signals with a g value of 1.98 to further proves the paramagnetic nature of Ti<sup>3+</sup> in the M-TiO<sub>2</sub>. XPS results also revealed the existence of defects in M-TiO<sub>2</sub> (Fig. S2d). M-TiO<sub>2</sub> showed significantly higher photocatalytic activity towards MB (Fig. S2e) and MO (Fig. S2f) degradation under visible light irradiation as compared to P-TiO<sub>2</sub>, which was attributed to the presence of defects.

All the above characterization techniques presented here clearly show that defects existed in M-TiO<sub>2</sub>.<sup>13</sup> In this study, we used this defective TiO<sub>2</sub> to further synthesize the Au/M-TiO<sub>2</sub> nanocomposite.

### Proposed mechanism for the formation of the Au/P-TiO<sub>2</sub> and Au/M-TiO<sub>2</sub> nanocomposites

The EAB was used for the synthesis of Au/P-TiO<sub>2</sub> and Au/M-TiO<sub>2</sub> nanocomposites, which is a green, cost-effective, surfactant-free, environmental-friendly, and mild-condition synthetic method. Fig. 1 presents the synthesis process of Au/P-TiO<sub>2</sub> or Au/M-TiO<sub>2</sub> nanocomposites. The EAB provides an excess of electrons and protons by biologically decomposing sodium acetate under anaerobic conditions.<sup>27-29</sup> The electrons produced by the EAB are responsible for the reduction of Au<sup>3+</sup> ions to Au<sup>0</sup> at the surface of the TiO<sub>2</sub> nanoparticles, which leads to the formation of Au/P-TiO<sub>2</sub> and Au/M-TiO<sub>2</sub> nanocomposites (Fig. 1). Furthermore, anchoring of AuNPs at the surface of TiO<sub>2</sub> occurred in the absence of surfactant or any other organic ligands. Generally, surfactants or organic ligand are used in the synthesis of metal-metal oxide nanocomposites and it is difficult to completely remove them from the final products and may remain at the interface of metal-metal oxide nanocomposites which generally forms an insulating layer and therefore prevents the formation of effective Schottky junction.<sup>26</sup> The advantage of this synthesis to fabricate Au/M-TiO<sub>2</sub> nanocomposite without any surfactant or organic ligand, facilitates the formation of effective Schottky junction. This is favorable for the effective charge carrier transfer through this Schottky junction during the photocatalytic process.<sup>26</sup> This reaction normally occurs in water at room temperature, which indicates the feasibility of this method for the preparation of a range of nanocomposite materials.

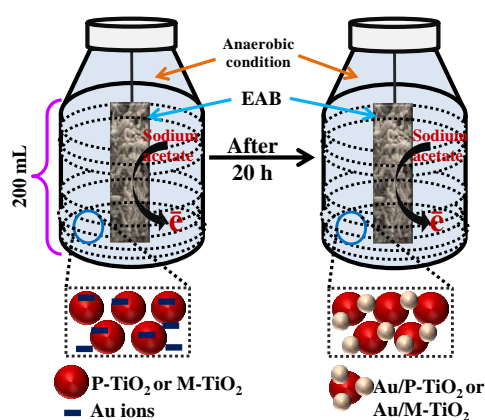


**Fig. 1** Proposed schematic diagram of the preparation of Au/P-TiO<sub>2</sub> and Au/M-TiO<sub>2</sub> nanocomposites using an EAB.

### Structural study

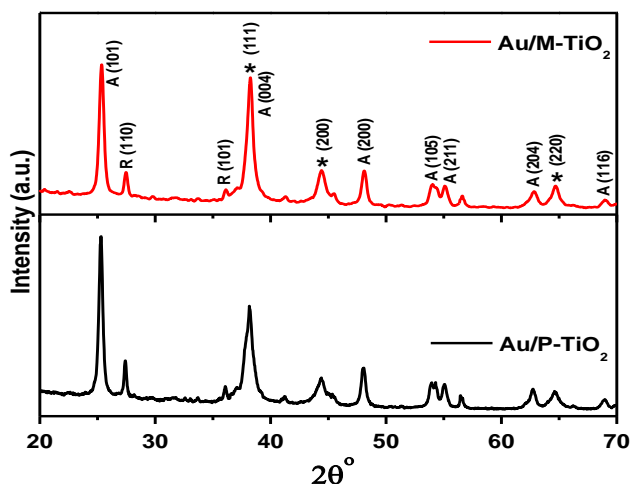


**Fig. 2** XRD patterns of the Au/P-TiO<sub>2</sub> and Au/M-TiO<sub>2</sub> nanocomposites. The peaks marked with (\*) were assigned to AuNPs.

The phase structures of the Au/P-TiO<sub>2</sub> and Au/M-TiO<sub>2</sub> nanocomposites were examined by XRD (Fig. 2). The unmarked XRD patterns of TiO<sub>2</sub> in both the Au/P-TiO<sub>2</sub> and Au/M-TiO<sub>2</sub> nanocomposites showed an identical crystal structure to that of pure TiO<sub>2</sub>.<sup>13</sup> The (101), (110), (101), (004), (200), (105), (211), (204) and (116) diffraction patterns corresponds to the anatase and rutile phase of TiO<sub>2</sub>.<sup>13,15</sup> The XRD patterns of anatase and rutile phase of TiO<sub>2</sub> were similar to that reported in the JCPDS file No. 73-1764 and 76-318, respectively. The XRD peaks at 38.2° (111), 44.38° (200) and 64.7° 2θ (220) are characteristic of face centered cubic gold, indicating the successful formation of AuNPs.<sup>22</sup> The peak of AuNPs at 38.2° 2θ overlapped with the peak for TiO<sub>2</sub>, resulting in a slight increase in the peak intensity.<sup>30</sup> The XRD pattern also confirmed the formation of AuNPs at the TiO<sub>2</sub> surface and overall formation of Au/P-TiO<sub>2</sub> and Au/M-TiO<sub>2</sub> nanocomposites. The crystallite sizes were calculated using Scherrer's equation and the calculated sizes for the Au/P-TiO<sub>2</sub> and Au/M-TiO<sub>2</sub> nanocomposites were ~18.76 and ~19.10 nm, respectively.<sup>9</sup> Further observations suggested that there

were no obvious changes in the XRD patterns of the Au/P-TiO<sub>2</sub> and Au/M-TiO<sub>2</sub> nanocomposites, suggesting that the anchoring of AuNPs does not affect the crystalline properties of the TiO<sub>2</sub>. These results further confirmed that the AuNPs were anchored successfully to the TiO<sub>2</sub> surface.

### Optical properties

The light absorption property of the metal and metal-metal oxide nanocomposites plays an important role in the utilization of visible light for a range of applications.<sup>9,11,12,22</sup> Fig. S2b shows the absorption spectra of the P-TiO<sub>2</sub> and M-TiO<sub>2</sub>. The absorption spectra reveal the M-TiO<sub>2</sub> to have significantly higher absorption in the visible light region. The band gap of the P-TiO<sub>2</sub> and M-TiO<sub>2</sub> was estimated directly from the absorption spectra, and found to be ~2.85 eV for the M-TiO<sub>2</sub>, which was red shifted compared to the P-TiO<sub>2</sub> ( $E_g = 3.10$  eV). The observed band gap of the M-TiO<sub>2</sub> was substantially smaller than that of the P-TiO<sub>2</sub> and was attributed to the presence of defects in M-TiO<sub>2</sub>.<sup>13,15</sup> The optical properties of the Au/P-TiO<sub>2</sub> and Au/M-TiO<sub>2</sub> nanocomposites were examined by UV-visible diffuse absorption/reflectance spectroscopy. Fig. 3a and S3 shows the absorption and reflectance spectra of the Au/P-TiO<sub>2</sub> and Au/M-TiO<sub>2</sub> nanocomposites. The absorption spectra of both Au/P-TiO<sub>2</sub> and Au/M-TiO<sub>2</sub> nanocomposites is dominated mainly by the broad absorption in the range, 500-600 nm, which was attributed to the SPR effect of AuNPs deposited on the TiO<sub>2</sub> surface.<sup>23,30</sup> The SPR effect of the AuNPs also serves as sensitizer to increase the visible light absorption by P-TiO<sub>2</sub> and M-TiO<sub>2</sub>, thereby improving their photocatalytic activities under visible light irradiation.<sup>31</sup> On the other hand, compared to the Au/P-TiO<sub>2</sub> nanocomposite, the Au/M-TiO<sub>2</sub> nanocomposite showed much higher absorption, which might be due to a combination of the SPR effect of AuNPs with the defect-induced narrow band gap of M-TiO<sub>2</sub>.<sup>13,15,16</sup>

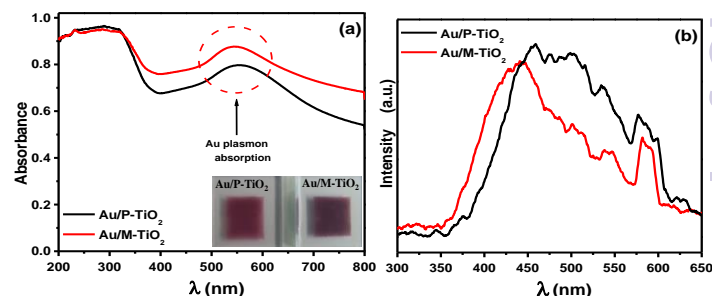


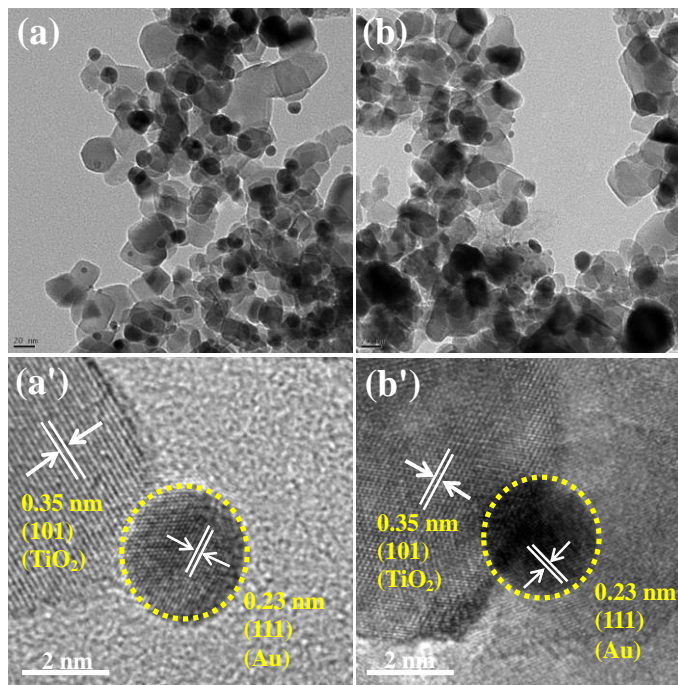
**Fig. 3** (a) UV-vis diffuse absorption spectra, and (b) PL spectra of Au/P-TiO<sub>2</sub> and Au/M-TiO<sub>2</sub> nanocomposites.

PL spectroscopy has been used widely to investigate the charge separation/recombination of photoinduced charge carriers (electron-hole pairs) in the materials.<sup>9,15,23</sup> In addition, the PL emission intensity is related directly to the recombination rate of the photoinduced electron-hole pairs, i.e., the lower the PL emission intensity, the lower the recombination rate of photoinduced electron-hole pairs, hence an increase in the photocatalytic activity of the materials.<sup>15,23,32</sup> Fig. 3b presents the PL emission spectra of the Au/P-TiO<sub>2</sub> and Au/M-TiO<sub>2</sub> nanocomposites. The Au/M-TiO<sub>2</sub> nanocomposite showed weaker emission intensity compared to the

Au/P-TiO<sub>2</sub> nanocomposite, which is related to the lower recombination rate of the photoinduced charge carriers in a Au/M-TiO<sub>2</sub> nanocomposite. This might be due to the presence of AuNPs and defects in M-TiO<sub>2</sub>, which quenches the PL emission of the Au/M-TiO<sub>2</sub> nanocomposite. This favors its high photocatalytic activity by prolonging the electron-hole pair lifetime.<sup>32,33</sup> In addition, the PL emission spectrum of the Au/M-TiO<sub>2</sub> nanocomposite shows a small blue shift compared to the Au/P-TiO<sub>2</sub> nanocomposite, which is similar to a previous report.<sup>34</sup> This shift was attributed to the anchoring of AuNPs to the M-TiO<sub>2</sub> surface and the interfacial interaction of AuNPs with M-TiO<sub>2</sub>.<sup>34</sup>

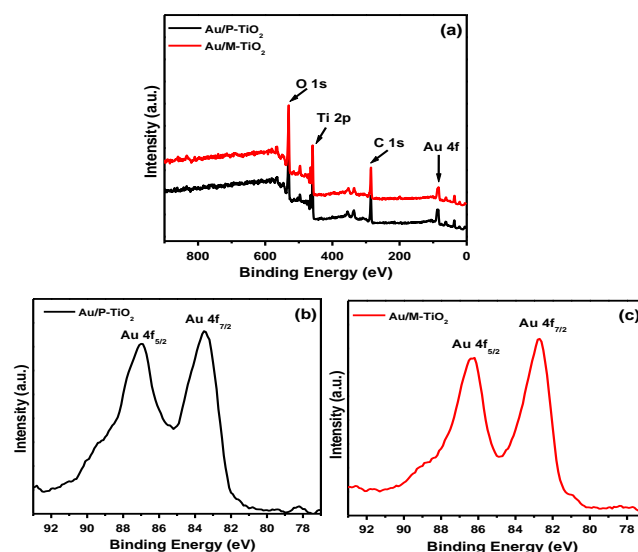
### Morphological and compositional studies

Fig. 4a and 4b present TEM image of the as-prepared Au/P-TiO<sub>2</sub> and Au/M-TiO<sub>2</sub> nanocomposites, which clearly shows the well dispersed AuNPs over the surface of the TiO<sub>2</sub> nanoparticle. The HRTEM image of the Au/P-TiO<sub>2</sub> (Fig. 4a') and Au/M-TiO<sub>2</sub> (Fig. 4b') nanocomposites revealed AuNP sizes of ~6-11 nm. In addition, the lattice fringe spacing of ~0.23 and ~0.35 nm, corresponds to the 111 plane of AuNPs and the 101 plane of the TiO<sub>2</sub>.<sup>13,23</sup> The SAED pattern shown in Fig. S4 and S5 shows that the nanocomposites (Au/P-TiO<sub>2</sub> and Au/M-TiO<sub>2</sub>) are crystalline in nature. Fig. S6 and S7 present the HAADF-STEM images of the Au/P-TiO<sub>2</sub> and Au/M-TiO<sub>2</sub> nanocomposites. EDS (Fig. S8 and S9) showed all the elemental compositions of the Au/M-TiO<sub>2</sub> nanocomposites corresponded to Ti, O and Au. TEM analysis further confirms the existence of AuNPs on the TiO<sub>2</sub> surface and interfacial interaction between the AuNPs and TiO<sub>2</sub>.



**Fig. 4** TEM and HRTEM images of the Au/P-TiO<sub>2</sub> (a and a') and Au/M-TiO<sub>2</sub> nanocomposites (b and b').

The surface composition and chemical state of the Au/P-TiO<sub>2</sub> and Au/M-TiO<sub>2</sub> nanocomposites were investigated by XPS. Fig. 5a shows the fully scanned spectra (survey) of the Au/P-TiO<sub>2</sub> and Au/M-TiO<sub>2</sub> nanocomposites, which confirms the presence of Ti, O, C, and Au. The C 1s photoelectron peak (Fig. S10) intensity for Au/P-TiO<sub>2</sub> and Au/M-TiO<sub>2</sub> nanocomposites was almost similar which indicates that no additional carbon was added via the EAB support during the synthesis process. This also suggests that the EAB was strongly adhered to the support and the biofilm was highly stable.<sup>28</sup>



**Fig. 5** XPS spectra of Au/P-TiO<sub>2</sub> and Au/M-TiO<sub>2</sub> nanocomposites (a) survey spectra, (b) Au 4f peak of Au/P-TiO<sub>2</sub> nanocomposite, and (c) Au 4f peak of Au/M-TiO<sub>2</sub> nanocomposite.

The Au 4f high resolution spectra of the Au/P-TiO<sub>2</sub> and Au/M-TiO<sub>2</sub> nanocomposites also confirmed the presence of AuNPs (Fig. 5b and 5c). The binding energy (BE) of the two individual peaks located at  $83.32 \pm 0.02$  and  $86.82 \pm 0.02$  eV for the Au/P-TiO<sub>2</sub> nanocomposite and  $82.76 \pm 0.02$  and  $86.31 \pm 0.02$  eV for Au/M-TiO<sub>2</sub> nanocomposite were assigned to the Au 4f<sub>7/2</sub> and Au 4f<sub>5/2</sub> of the AuNPs, respectively. These doublet peaks suggested the presence of metallic Au in the Au/P-TiO<sub>2</sub> and Au/M-TiO<sub>2</sub> nanocomposites.<sup>35</sup> In addition, the BE of Au 4f<sub>7/2</sub> and Au 4f<sub>5/2</sub> in Au/P-TiO<sub>2</sub> and Au/M-TiO<sub>2</sub> nanocomposites shifted to a lower value compared to pure metallic Au (BE of metallic Au is ~84.0 eV for Au 4f<sub>7/2</sub> and ~87.7 eV for Au 4f<sub>5/2</sub>), which also supports the interfacial interactions between the AuNPs and TiO<sub>2</sub> nanoparticles.<sup>35,36</sup> Moreover, the BE of Au 4f in the Au/M-TiO<sub>2</sub> nanocomposite shifted to a lower value compared to the Au/P-TiO<sub>2</sub> nanocomposite. This lower shift of the BE in the case of the Au/M-TiO<sub>2</sub> nanocomposite was assigned to the strong interfacial interaction between AuNPs and defective sites on the surface of M-TiO<sub>2</sub>.<sup>36</sup>

### Visible light driven photocatalytic degradation of MB, MO and 2-CP

The effects of the SPR phenomena of AuNPs on the visible light activity of the P-TiO<sub>2</sub> and M-TiO<sub>2</sub> were studied systematically by photocatalytic and photoelectrochemical experiments. Generally, a dye degradation experiment is used widely as a model reaction to evaluate the photocatalytic activities of various photocatalysts.<sup>1,7,9-11</sup> The photocatalytic activities of Au/P-TiO<sub>2</sub> and Au/M-TiO<sub>2</sub> nanocomposites were evaluated by the degradation of colored dyes (MB and MO) and non-colored organic compound 2-CP under visible light irradiation. Fig. 6a and 6b presents the degradation kinetics plot of the MB and MO whereas Fig. S11a and S11b show the C/C<sub>0</sub> vs. time plot of the MB and MO degradation as a function of the irradiation time.<sup>9,15</sup> The change in the concentration of MB and MO as a function of the reaction time for the Au/P-TiO<sub>2</sub> and Au/M-TiO<sub>2</sub> nanocomposites exhibited pseudo-first-order kinetics according to the equation reported elsewhere.<sup>25</sup> The rate constants (*k*) of the Au/P-TiO<sub>2</sub> and Au/M-TiO<sub>2</sub> nanocomposites for the degradation of MB were 0.2577/h (*R*<sup>2</sup> = 0.9884) and 0.4669/h (*R*<sup>2</sup> = 0.9872), respectively. Similarly, the rate constants of the Au@P-TiO<sub>2</sub> and Au@M-TiO<sub>2</sub> nanocomposites for the degradation of MO were 0.06934/h (*R*<sup>2</sup> = 0.9964) and 0.1631/h (*R*<sup>2</sup> = 0.9884), respectively. The *k* value for the photocatalytic degradation of MB and MO by the Au/M-TiO<sub>2</sub> nanocomposite was ~2 and 2.4 times higher than that of Au/P-TiO<sub>2</sub> nanocomposite. As shown in Fig. S11a and S11b, the Au/M-TiO<sub>2</sub> nanocomposite exhibited much higher photocatalytic activity than the P-TiO<sub>2</sub> and M-TiO<sub>2</sub> nanoparticles and the Au/P-TiO<sub>2</sub> nanocomposite under visible light irradiation.<sup>13</sup> The photocatalytic activity of P-TiO<sub>2</sub> and M-TiO<sub>2</sub> have been reported previously, in which after 6 and 8 h of visible light irradiation ~88% of MB and ~42% of MB degradation was achieved by M-TiO<sub>2</sub> (Fig. S2e and S2f).<sup>13</sup> However, Au/M-TiO<sub>2</sub> nanocomposite showed ~96% and ~74% degradation efficiencies of the MB and MO dye after 6 and 8 h of visible light irradiation, respectively, whereas Au/P-TiO<sub>2</sub> showed only ~80% and ~44% degradation efficiency for MB and MO after 6 and 8 h of visible light irradiation, respectively.

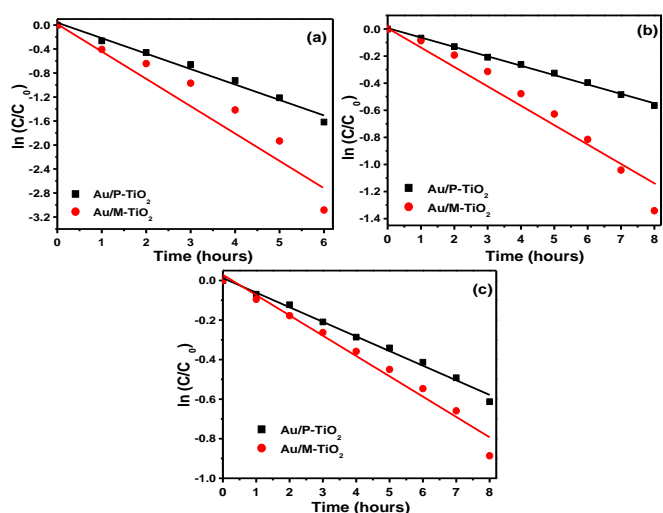


**Fig. 6**  $\ln(C/C_0)$  versus time (h) plot for the photodegradation of (a) MB, (b) MO, and (c) 2-CP by Au/P-TiO<sub>2</sub> and Au/M-TiO<sub>2</sub> nanocomposites under visible light irradiation.

The photocatalytic degradation of non-colored 2-CP, which did not absorb the light in the visible region, was also performed under visible light irradiation (Fig. S11c). Under visible light irradiation, the Au/M-TiO<sub>2</sub> nanocomposite exhibited excellent photodegradation ability for the degradation of 2-CP compared to the P-TiO<sub>2</sub> and M-TiO<sub>2</sub> nanoparticles and the Au/P-TiO<sub>2</sub> nanocomposite because of the characteristic SPR absorption of AuNPs and the narrowed band gap of M-TiO<sub>2</sub>. Fig. 6c shows the photocatalytic degradation kinetic plot of 2-CP. The *k* value of the Au/P-TiO<sub>2</sub> and Au/M-TiO<sub>2</sub> nanocomposites for the degradation of 2-CP were 0.07385/h (*R*<sup>2</sup> = 0.9920) and 0.1026/h (*R*<sup>2</sup> = 0.9870). The *k* value for the photocatalytic degradation of 2-CP by the Au/M-TiO<sub>2</sub> nanocomposite was ~1.4 times higher than that of Au/P-TiO<sub>2</sub> nanocomposite. In addition, photodegradation efficiency obtained in this case was also much higher than that previously reported for metal oxides (TiO<sub>2</sub>, ZnO and CeO<sub>2</sub>), suggesting the suitability of the Au/M-TiO<sub>2</sub> nanocomposite for environmental remediation processes.<sup>9,13,15,23</sup>

The stability of the Au/P-TiO<sub>2</sub> and Au/M-TiO<sub>2</sub> nanocomposites without the leaching of AuNPs is an important concern, which further determines the usability of the catalyst for a range of reaction conditions. Stability tests were conducted by sonicating the Au/P-TiO<sub>2</sub> and Au/M-TiO<sub>2</sub> photocatalysts in water for one hour. The centrifuged solution was analyzed for any leached AuNPs using an UV-visible spectrophotometer. The absorption spectra of the centrifuged solution of Au/P-TiO<sub>2</sub> and Au/M-TiO<sub>2</sub> (Fig. S12 and S13) showed no absorbance peak in the range, 500-600 nm, corresponding to the AuNPs. This confirms that the AuNPs are strongly anchored to the TiO<sub>2</sub> surface and are stable. This analysis confirms the stability of the as-prepared Au/P-TiO<sub>2</sub> and Au/M-TiO<sub>2</sub> nanocomposites.

### Proposed mechanism for the photocatalytic degradation of MB, MO and 2-CP under visible light irradiation

Fig. 7 presents the possible photoexcitation and electron transfer mechanism for the photocatalytic activities of Au/P-TiO<sub>2</sub> and Au/M-TiO<sub>2</sub> nanocomposites under visible light irradiation. In the case of Au/P-TiO<sub>2</sub> (Fig. 7a), the generation of electrons in the conduction bands and holes in the valence bands under visible light is not a feasible process because of the wide band gap of P-TiO<sub>2</sub> (Fig. 7a).<sup>10</sup> In contrast, Au/P-TiO<sub>2</sub> exhibited little photocatalytic activity due to photon absorption by the SPR effect of AuNPs under visible light irradiation.<sup>11,12,22</sup>

On the other hand, in the case of Au/M-TiO<sub>2</sub> (Fig. 7b), M-TiO<sub>2</sub> has a narrower band gap, which results in greater visible light absorption, and photon absorption also occurs due to the SPR phenomena of AuNPs.<sup>22,24</sup> The combined effect of these two processes results in much higher visible light absorption, hence an increase in photocatalytic activity. When Au/M-TiO<sub>2</sub> is irradiated with visible light, the electrons in M-TiO<sub>2</sub> migrate from the valence band to the conduction band, as evident from Fig. 7b,<sup>14,15,17,19</sup> and the AuNPs are photoexcited by the SPR phenomenon, leading to the generation of electrons and holes.<sup>24,35</sup> The photoexcited electrons are injected into the conduction band of the M-TiO<sub>2</sub> nanoparticles leaving behind holes in the AuNPs.<sup>35</sup> The excess of

photogenerated electrons on the surface of the Au/M-TiO<sub>2</sub> nanocomposite due to the above mentioned process are then scavenged by surface adsorbed oxygen to yield highly oxidative species, such as  $\cdot\text{O}_2^-$  and  $\text{HO}\cdot$  radicals.<sup>6,8,9</sup> The positive holes in the AuNPs and M-TiO<sub>2</sub> are trapped by OH<sup>-</sup> species to yield reactive HO<sup>+</sup> radicals. These reactive radicals are responsible for the degradation and mineralization of MB, MO and 2-CP.<sup>5,8,10,36</sup> Therefore, with the synergetic effect of the narrow band gap of M-TiO<sub>2</sub> and the SPR phenomena of AuNPs, a large number of photogenerated electrons and holes are produced and separated, which participate in the photodegradation process leading to an increase in photocatalytic activity.

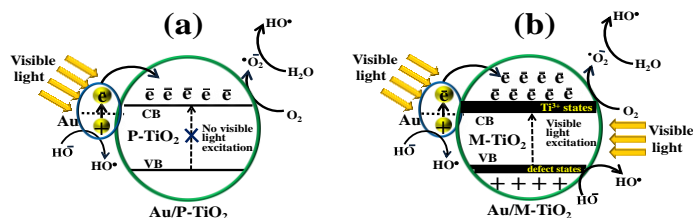


**Fig. 7** Schematic diagram of the proposed mechanism for the degradation of MB, MO and 2-CP by (a) Au/P-TiO<sub>2</sub>, and (b) Au/M-TiO<sub>2</sub> nanocomposite under visible light irradiation.

### Photoelectrochemical Studies

The charge transfer resistance and separation efficiency of the photogenerated charge carriers across the Au/P-TiO<sub>2</sub> and Au/M-TiO<sub>2</sub> nanocomposites photoelectrodes were examined by EIS.<sup>9,15</sup> Generally, the semicircular arc in the EIS spectra is an expression of the magnitude of the charge transfer resistance at the photoelectrode/electrolyte interface.<sup>23,35</sup> In other words, the smaller the arc radius, smaller the charge transfer resistance and the higher the charge separation efficiency, which leads to higher photoactivity of the photoelectrodes.<sup>22,35</sup> Fig. 8a and 8b presents the EIS spectra of the P-TiO<sub>2</sub> and the Au/P-TiO<sub>2</sub> and M-TiO<sub>2</sub> nanoparticles Au/M-TiO<sub>2</sub> nanocomposites photoelectrodes in the dark and under visible light irradiation. As shown in the Fig., Au/M-TiO<sub>2</sub> nanocomposite photoelectrode has a much smaller arc radius than the Au/P-TiO<sub>2</sub> nanocomposite, P-TiO<sub>2</sub> and M-TiO<sub>2</sub> nanoparticles. These results suggest that the Au/M-TiO<sub>2</sub> nanocomposite has a lower resistance to interfacial charge transfer. Therefore, the effective separation of photogenerated electron hole pairs occurs under visible light irradiation.<sup>23,37</sup> Overall, the significant enhancement in the photoelectrochemical performance of the Au/M-TiO<sub>2</sub> nanocomposite is due to the synergistic effects of AuNPs and defect-induced narrow band gap of M-TiO<sub>2</sub>. These results are in accordance with the photodegradation results of the Au/M-TiO<sub>2</sub> nanocomposite.

In addition to the photodecomposition process, the charge carriers accumulated on the surface of the photocatalyst are also responsible for inducing charging behavior in the materials.<sup>37-38</sup> Therefore, in this case, the charging behavior of the Au/P-TiO<sub>2</sub> and Au/M-TiO<sub>2</sub> nanocomposites was analyzed further by DPV.<sup>39</sup> Fig. 8c and 8d presents the DPV responses of the P-TiO<sub>2</sub> and M-TiO<sub>2</sub> nanoparticles and the Au/P-TiO<sub>2</sub> and Au/M-TiO<sub>2</sub> nanocomposites

under visible light irradiation. Au/P-TiO<sub>2</sub> and Au/M-TiO<sub>2</sub> nanocomposites showed well-defined quantized capacitance charging peaks in the dark and under visible light irradiation at -0.43 V. In addition, the Au/M-TiO<sub>2</sub> nanocomposite under visible light irradiation also exhibited enhanced and excellent charge storage properties compared to P-TiO<sub>2</sub>, M-TiO<sub>2</sub> and Au/P-TiO<sub>2</sub>. This enhanced performance of Au/M-TiO<sub>2</sub> might be due to the synergistic effects of AuNPs and the defect-induced narrow band gap of M-TiO<sub>2</sub>.

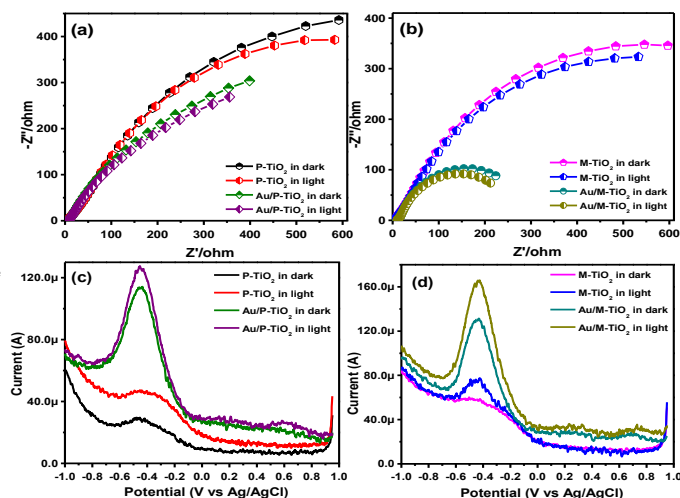


**Fig. 8** EIS spectra (a and b) and DPV (c and d) obtained for the Au/P-TiO<sub>2</sub> and Au/M-TiO<sub>2</sub> nanocomposites photoelectrodes in the dark and under visible light irradiation.

### Conclusions

AuNPs-sensitized wide band gap TiO<sub>2</sub> (Au/P-TiO<sub>2</sub>) and narrow band gap TiO<sub>2</sub> (Au/M-TiO<sub>2</sub>) were prepared using an electrochemically active biofilm. The photosensitization property of the Au nanoparticles enhanced the absorption of TiO<sub>2</sub> over the broad visible region by acting as light harvesters. As a result, the Au/P-TiO<sub>2</sub> and Au/M-TiO<sub>2</sub> nanocomposites promoted the photocatalytic degradation efficiency of methylene blue, methyl orange and 2-chlorophenol under visible light irradiation. In addition, Au/M-TiO<sub>2</sub> nanocomposite showed much higher photodegradation ability than the P-TiO<sub>2</sub> and M-TiO<sub>2</sub> nanoparticles and the Au/P-TiO<sub>2</sub> nanocomposite. Furthermore, the electrochemical impedance spectroscopy and differential pulse voltammetry response of the Au/M-TiO<sub>2</sub> nanocomposite under visible light irradiation showed enhanced performance compared to the P-TiO<sub>2</sub> and M-TiO<sub>2</sub> nanoparticles and Au/P-TiO<sub>2</sub> nanocomposite. These enhanced photocatalytic degradation efficiencies and photoelectrochemical performance were attributed mainly to the surface plasmon resonance effect of the Au nanoparticles excited by visible light irradiation. In addition, the presence of a defect-induced narrowed band gap M-TiO<sub>2</sub> in the Au/M-TiO<sub>2</sub> nanocomposite contributes to higher photocatalytic activities. Owing to the ease of preparation of these materials by a simple, novel and green route as well as high photocatalytic activities, Au/M-TiO<sub>2</sub> nanocomposite can be applied to a wide range of processes that may lead to its commercialization.

## Acknowledgements

This study was supported by Priority Research Centers Program through the National Research Foundation of Korea (NRF) funded by the Ministry of Education (2014R1A6A1031189).

## Notes and references

<sup>a</sup>School of Chemical Engineering, Yeungnam University, Gyeongsan-si, Gyeongbuk 712-749, South Korea. Phone: +82-53-810-2517; Fax: +82-53-810-4631.

<sup>b</sup>Chemical Sciences, Faculty of Science, Universiti Brunei Darussalam, Jalan Tungku Link, BE1410, Brunei Darussalam.

### \*Corresponding authors

Email: mhcho@ynu.ac.kr; mmansoobkhan@yahoo.com

†Electronic Supplementary Information (ESI) available: [Schematic diagram of the photoelectrochemical measurement, characterization and photodegradation results of P-TiO<sub>2</sub> and M-TiO<sub>2</sub>, DRS, SAED, HAADF, EDX, C 1s spectra, photocatalytic degradation plots of MB, MO & 2-CP and stability test spectra of Au/P-TiO<sub>2</sub> and Au/M-TiO<sub>2</sub> nanocomposites] See DOI: 10.1039/b000000x/

- 1 T. Sakamoto, D. Nagao, M. Noba, H. Ishii, and M. Konno, *Langmuir*, 2014, **30**, 7244–7250.
- 2 Q. Li, N. Zhang, Y. Yang, G. Wang and D. H. L. Ng, *Langmuir*, 2014, **30**, 8965–8972.
- 3 F. M. Machado, C. P. Bergmann, E. C. Lima, B. Royer, F. E. de Souza and I. M. Jauris, *Phys. Chem. Chem. Phys.*, 2012, **14**, 11139–11153.
- 4 B. Chen, X. Wang, C. Wang, W. Jiang and S. Li, *Ultrasonics Sonochemistry*, 2011, **18**, 1091–1096.
- 5 Y. Ma, X. Wang, Y. Jia, X. Chen, H. Han and Can Li, *Chem. Rev.*, 2014, **114**, 9987–10043.
- 6 J. Ran, J. Zhang, J. Yu, M. Jaroniec and S. Z. Qiao, *Chem. Soc. Rev.*, 2014, **43**, 7787–7812.
- 7 A. B. Djurić, Y. H. Leung and A. M. Ching Ng, *Mater. Horiz.*, 2014, **1**, 400–410.
- 8 S. Banerjee, S. C. Pillai, P. Falaras, K. E. O'Shea, J. A. Byrne and D. D. Dionysiou, *J. Phys. Chem. Lett.*, 2014, **5**, 2543–2554.
- 9 S. A. Ansari, M. M. Khan, M. O. Ansari, J. Lee and M. H. Cho, *J. Phys. Chem. C*, 2013, **117**, 27023–27030.
- 10 A. Ajmal, I. Majeed, R. N. Malik, H. Idriss and M. A. Nadeem, *RSC Adv.*, 2014, **4**, 37003–37026.
- 11 H. Wang, L. Zhang, Z. Chen, J. Hu, S. Li, Z. Wang, J. Liu and X. Wang, *Chem. Soc. Rev.*, 2014, **43**, 5234–5244.
- 12 S. T. Kochuveedu, Y. H. Jang and D. H. Kim, *Chem. Soc. Rev.*, 2013, **42**, 8467–8493.
- 13 S. Kalathil, M. M. Khan, S. A. Ansari, J. Lee and M. H. Cho, *Nanoscale*, 2013, **5**, 6323–6326.
- 14 X. Pan, M.-Q. Yang, X. Fu, N. Zhang and Y.-J. Xu, *Nanoscale*, 2013, **5**, 3601–3614.
- 15 M. M. Khan, S. A. Ansari, D. Pradhan, M. O. Ansari, D. H. Han, J. Lee and M. H. Cho, *J. Mater. Chem. A*, 2014, **2**, 637–644.
- 16 Q. Zhu, Y. Peng, L. Lin, C.-M. Fan, G.-Q. Gao, R.-X. Wang and A.-W. Xu, *J. Mater. Chem. A*, 2014, **2**, 4429–4437.
- 17 F. Zuo, L. Wang, T. Wu, Z. Y. Zhang, D. Borchardt and P. Y. Feng, *J. Am. Chem. Soc.*, 2010, **132**, 11856–11857.
- 18 X. B. Chen, L. Liu, P. Y. Yu and S. S. Mao, *Science*, 2011, **331**, 746–750.
- 19 I. Nakamura, N. Negishi, S. Kutsuna, T. Ihara, S. Sugihara and K. Takeuchi, *J. Mol. Catal. A: Chem.*, 2000, **161**, 205–212.
- 20 J. Jun, M. Dhayal, J. H. Shin, J. C. Kim and N. Getoff, *Rad. Phys. Chem.*, 2006, **75**, 583–589.
- 21 X. Chen, L. Liu, P. Y. Yu and S. S. Mao, *Science*, 2011, **331**, 746–750.
- 22 C. Wang and D. Astruc, *Chem. Soc. Rev.*, 2014, **43**, 7188–7216.
- 23 M. M. Khan, S. A. Ansari, M. O. Ansari, B. K. Min, J. Lee and M. H. Cho, *J. Phys. Chem. C*, 2014, **118**, 9477–9484.
- 24 C. Clavero, *Nature Photonics*, 2014, **8**, 95–103.
- 25 X. Pan and Y.-J. Xu, *Appl. Catal., A*, 2013, **459**, 34–40.
- 26 D. Ding, K. Liu, S. He, C. Gao and Y. Yin, *Nano Lett.*, 2014, **14**, 6731–6736.
- 27 M. M. Khan, S. Kalathil, T. H. Han, J. Lee and M. H. Cho, *J. Nanosci. Nanotechnol.*, 2013, **13**, 6079–6085.
- 28 M. M. Khan, S. A. Ansari, J. H. Lee, J. Lee and M. H. Cho, *ACS Sustainable Chem. Eng.*, 2014, **2**, 423–432.
- 29 T. H. Han, M. M. Khan, S. Kalathil, J. Lee and M. H. Cho, *Ind. Eng. Chem. Res.*, 2013, **52**, 8174–8181.
- 30 M. M. Khan, S. Kalathil, J. Lee, and M. H. Cho, *Bull. Korean Chem. Soc.*, 2012, **33**, 1753–1758.
- 31 C. Zhou, L. Shang, H. Yu, T. Bian, L.-Z. Wua, C.-H. Tung and T. Zhang, *Catalysis Today*, 2014, **225**, 158–163.
- 32 J. Liqiang, Q. Yichun, W. Baiqi, L. Shudan, J. Baojiang, Y. Libin, F. Wei, F. Honggang and S. Jiazhong, *Sol. Energy Mater. Sol. Cells*, 2006, **90**, 1773–1787.
- 33 A. Bumajdad and M. Madkour, *Phys. Chem. Chem. Phys.*, 2014, **16**, 7146–7158.
- 34 S. F. Chen, J. P. Li, K. Qian, W. P. Xu, Y. Lu, W. X. Huang and S. H. Yu, *Nano Res.*, 2010, **3**, 244–255.
- 35 Y. Wang, J. Yu, W. Xiao and Q. Lia, *J. Mater. Chem. A*, 2014, **2**, 3847–3855.
- 36 Z. Khan, T. R. Chetia and M. Qureshi, *Nanoscale*, 2012, **4**, 3543–3550.
- 37 X. Pan and Y.-J. Xu, *Appl. Catal., A*, 2013, **459**, 34–40.
- 38 R. W. Murray, *Chem. Rev.*, 2008, **108**, 2688–2720.
- 39 M. M. Khan, S. A. Ansari, J. Lee and M. H. Cho, *J. Ind. Eng. Chem.*, 2013, **19**, 1845–1850.